The nucleation rate of single O_2 nanobubbles at Pt nanoelectrodes

Álvaro Moreno Soto,*,†,‡ Sean R. German,† Hang Ren,† Devaraj van der Meer,‡ Detlef Lohse,*,‡ Martin A. Edwards,† and Henry S. White*,†

†*Department of Chemistry, University of Utah, 315 South 1400 East, 84112-0850, Salt Lake City, Utah, USA*

‡*Physics of Fluids Group and Max Planck Center Twente, MESA+ Institute and J. M. Burgers Centre for Fluid Dynamics, Faculty of Science and Technology, University of Twente, P.O. Box 217, 7500 AE Enschede, The Netherlands*

E-mail: a.morenosoto@utwente.nl; d.lohse@utwente.nl; white@chem.utah.edu

Supporting Information

Table of contents

1. Fabrication of nanoelectrodes

Nanoelectrodes were fabricated using a previously reported procedure,[1] shown schematically in Figure S1. Briefly, a Pt wire (Alfa Aesar) of 25 μm diameter was glued to a W rod (A-M Systems) using silver epoxy (Alfa Aesar). The wire was then inserted in a borosilicate glass capillary (Prism Glass Capillaries) of 0.5 mm inner diameter and 1.0 mm outer diameter, which serves to insulate the electrode. The Pt wire was then etched with sodium cyanide (6 M) to obtain a sharpened tip. The Pt wire and the W rod were afterwards sealed inside the glass capillary by heating with a hydrogen torch. Finally, a polishing process exposes the tip of the Pt nanowire, producing a Pt inlaid disk in the insulating glass plane.

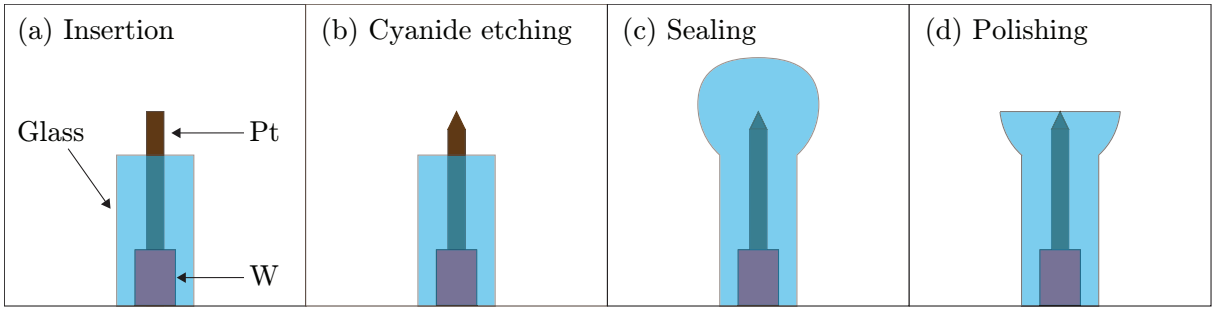

Figure S1: Fabrication of nanoelectrodes: (a) the Pt wire glued to a W rod is inserted into a glass capillary, (b) the Pt is etched by cyanide, achieving a pointed tip of nanometer size, (c) the Pt is sealed in the glass capillary by heating with a hydrogen torch, and (d) the seal is polished until exposure of the Pt tip.

The apparent size of the electrode was determined by measuring the limiting current for ferrocene oxidation to ferrocenium.[2–5] This method is reliable for nanodisk electrodes.[1] The diffusion limited current i_{lim} to a disk electrode is:

$$i_{\text{lim}} = 4nFD_{\text{Fc}}C_{\text{Fc}}a, \tag{1}$$

where $n = 1$ is the number of electrons exchanged, $F = 96485$ C/mol is Faraday's constant, $D_{\text{Fc}} = 2.4 \times 10^{-9}$ m^2/s is the ferrocene diffusivity,[6] $C_{\text{Fc}} = 5$ mM is the ferrocene bulk concentration and a is the apparent radius of the nanoelectrode. Voltammograms used to determine the size of the three nanoelectrodes used in the main text are presented in Figure

S2.

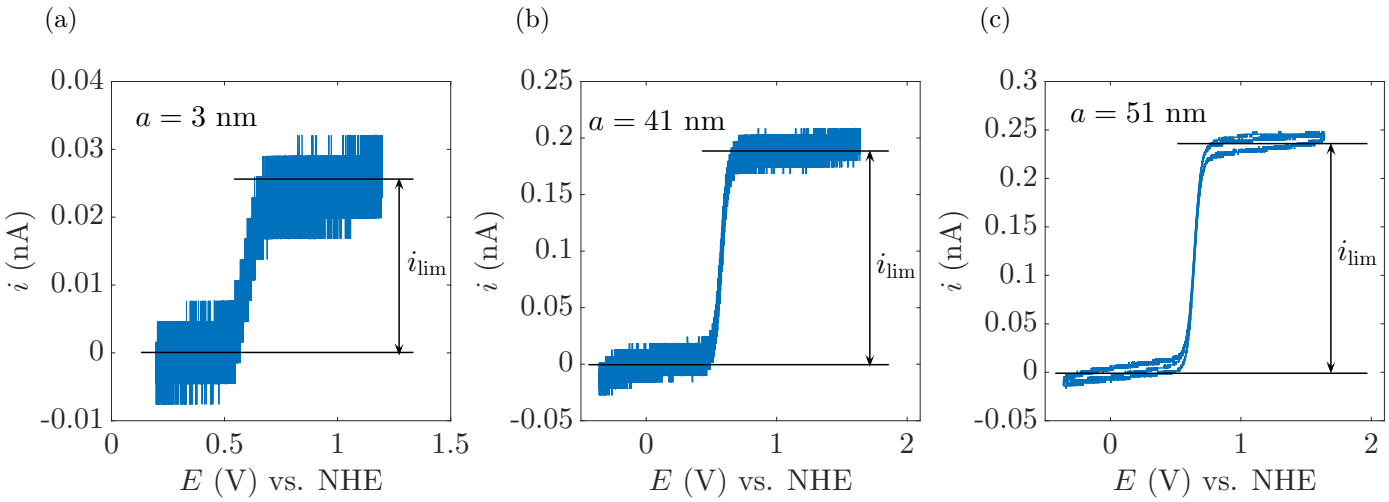

Figure S2: Voltammograms of ferrocene oxidation to ferrocenium used to measure the size of the nanoelectrodes. Note that the current scale is different on each plot. The solution contains 5 mM Fc and 0.1 M tetrabutylammonium hexaflurophosphate in acetonitrile.

Figure S3 shows the voltammograms before and after 50 nucleation cycles on conditioned and non-conditioned electrodes. On conditioned electrodes, Figure S3a, the voltammograms did not apparently differ, i.e. the apparent radius a remained constant throughout the nucleation cycles. That was not the case for the electrodes in which a conditioning cycle was not performed prior to the nucleation cycles, Figure S3b. In those situations, the electrode apparent radius could increase up to $\sim 5a$. This fact adds up to the surface chemistry affecting the reproducibility of peak current values $i_{\mathrm{nb}}^{\mathrm{p}}$, since $i_{\mathrm{nb}}^{\mathrm{p}}$ and a are directly proportional to each other.[4,7,8]

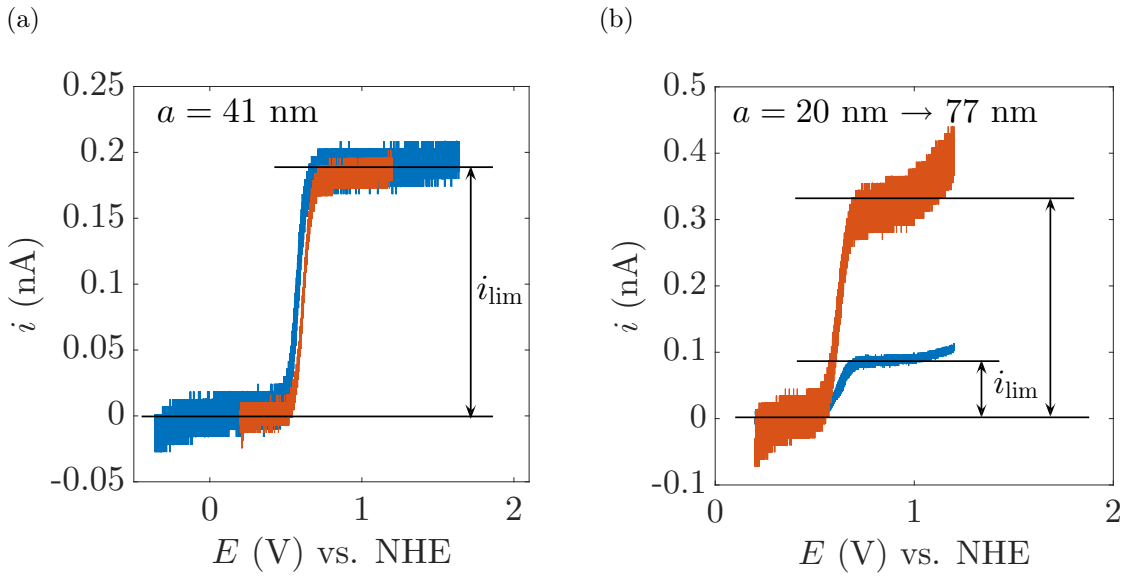

Figure S3: Voltammograms of ferrocene oxidation to ferrocenium used to measure the size of the nanoelectrodes before (blue) and after (red) 50 nucleation cycles. The solution contains 5 mM Fc and 0.1 M tetrabutylammonium hexaflurophosphate in acetonitrile. (a) On conditioned electrodes, the voltammograms remain the same, indicating that the apparent electrode radius a remains quasi-constant throughout the experiments. (b) On non-conditioned electrodes, a increases significantly and consequently, experiments performed with these electrodes result in non-reproducible peak current values $i_{\mathrm{nb}}^{\mathrm{p}}$ and nucleation times t_{ind}.

2. Nanoelectrode conditioning

Best reproducibility of i_{nb}^{p} was observed when great care was exercized to control the potential waveform prior to applying a current, i_{app}. This requirement is related to the formation and stripping of the surface oxide on Pt at potentials where H_2O_2 is oxidized.[9,10] As we discussed in the main text, at least 40 nanobubble nucleation repetitions need to be performed in order to achieve a reproducible peak current i_{nb}^{p}. To obtain reproducible results with lower standard deviation within fewer repetition, we designed a new potential waveform, in which we can control certain parameters, defined in the main text as t_{dis}, t_{stab}, E_{stab} and t_{rest} in Figure 5a. Figures S4a-e show the current response after 100 repetitions for different conditioning cycles corresponding to various combinations of those parameters. Figure S4f represents the evolution of i_{nb}^{p} with the number of nucleated bubbles for the different conditioning waveforms. We conclude that the best reproducibility is obtained with $t_{dis} = 1$ s, $t_{stab} = 2$ s, $E_{stab} = 0.89$ V, and $t_{rest} = 1$ s, corresponding to Figure S4d, green diamond curve in Figure S4f.

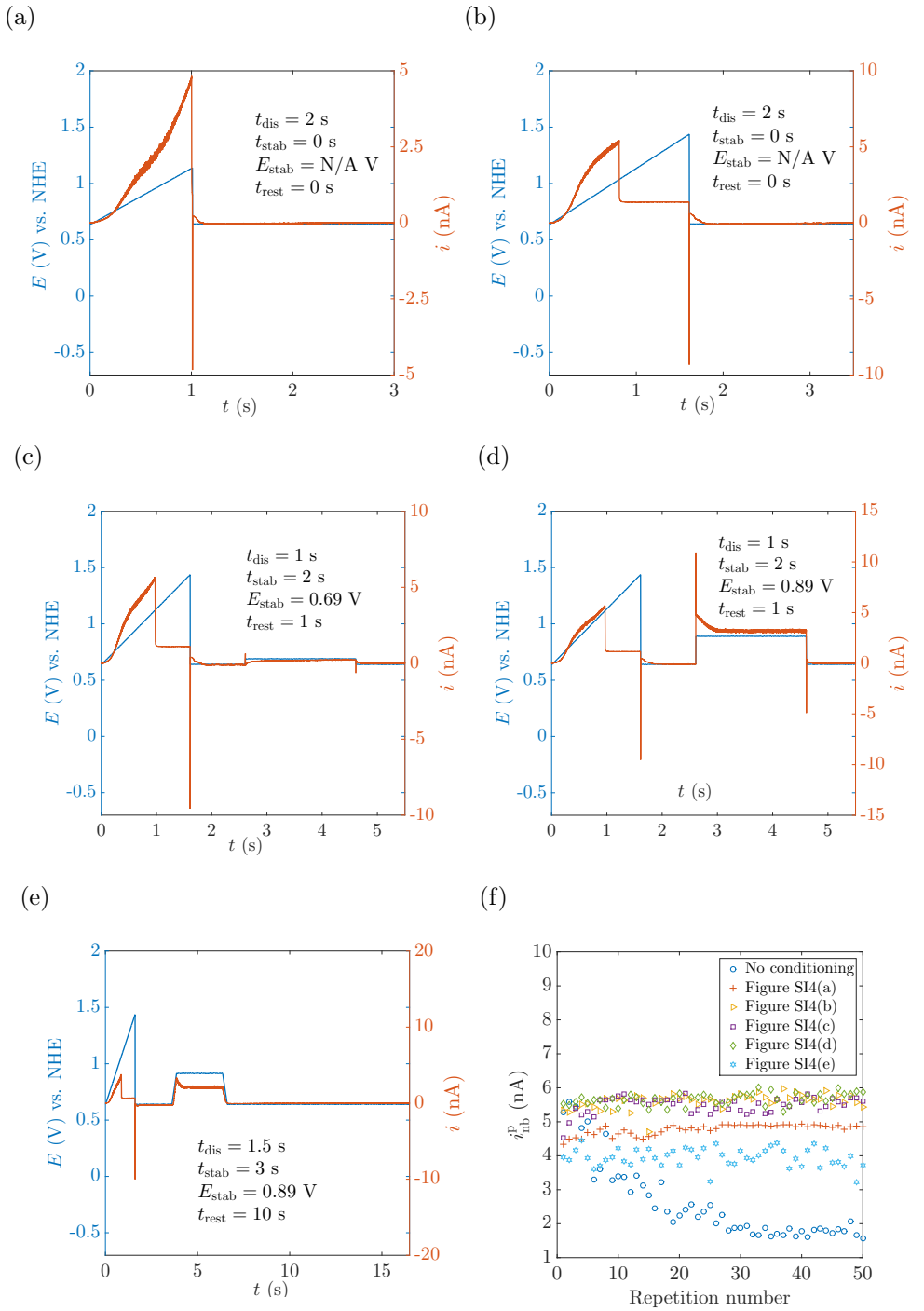

Figure S4: (a)-(e) Different electrode conditioning cycles. In blue, the controlled voltage is shown, whereas the red curve corresponds to the current response after 100 repetitions. The difference between panel (a) and (b) resides in the different nanobubble nucleation cycle: for the first case, the slope corresponds to $\Delta E = 0.5$ V in $t = 1$ s, whereas for the second case, and all other conditioning cycles, $\Delta E = 0.8$ V in $t = 1.6$ s. In panel (e), we used a ramp model to reach E_{stab} to avoid the sudden increase of current. The optimal empirical configuration corresponds to conditioning cycle (d). (f) Corresponding peak current i_{nb}^{p} for different conditioning procedures vs. the repetition number during conditioning.

3. Nucleation rate measurements for additional values of i_{app} and electrodes

A nanobubble nucleates almost immediately when $i_{\mathrm{nb}}^{\mathrm{p}}$ is reached. However, nanobubbles take a longer time to nucleate, grow, and block the electrode when a current i_{app}, whose value is very close to but lower than $i_{\mathrm{nb}}^{\mathrm{p}}$, is applied. The lower the i_{app} compared to $i_{\mathrm{nb}}^{\mathrm{p}}$, the longer it takes for nanobubbles to nucleate.[11] In the main text, several results of nucleation induction times for a 41 nm radius electrode are shown, Figure 7. Figure S5 shows the corresponding results of nucleation induction times for other current levels not shown in the main text. Figure S5a indicates the interval from which the nucleation time t_{ind} is measured. The interval begins at the moment in which the current is applied and ends at the moment in which the nanobubble nucleates (indicated by a large increase in the voltage as the bubble blocks the surface of the nanoelectrode).

Figures S6 and S7 show voltage-time responses for bubble nucleation for two different nanoelectrodes with corresponding apparent radii $a = 3$ and 51 nm, respectively. In Figures S8 and S9, we show the corresponding plots for t_{ind} as a function of i_{app} and the probability distribution P for these electrodes.

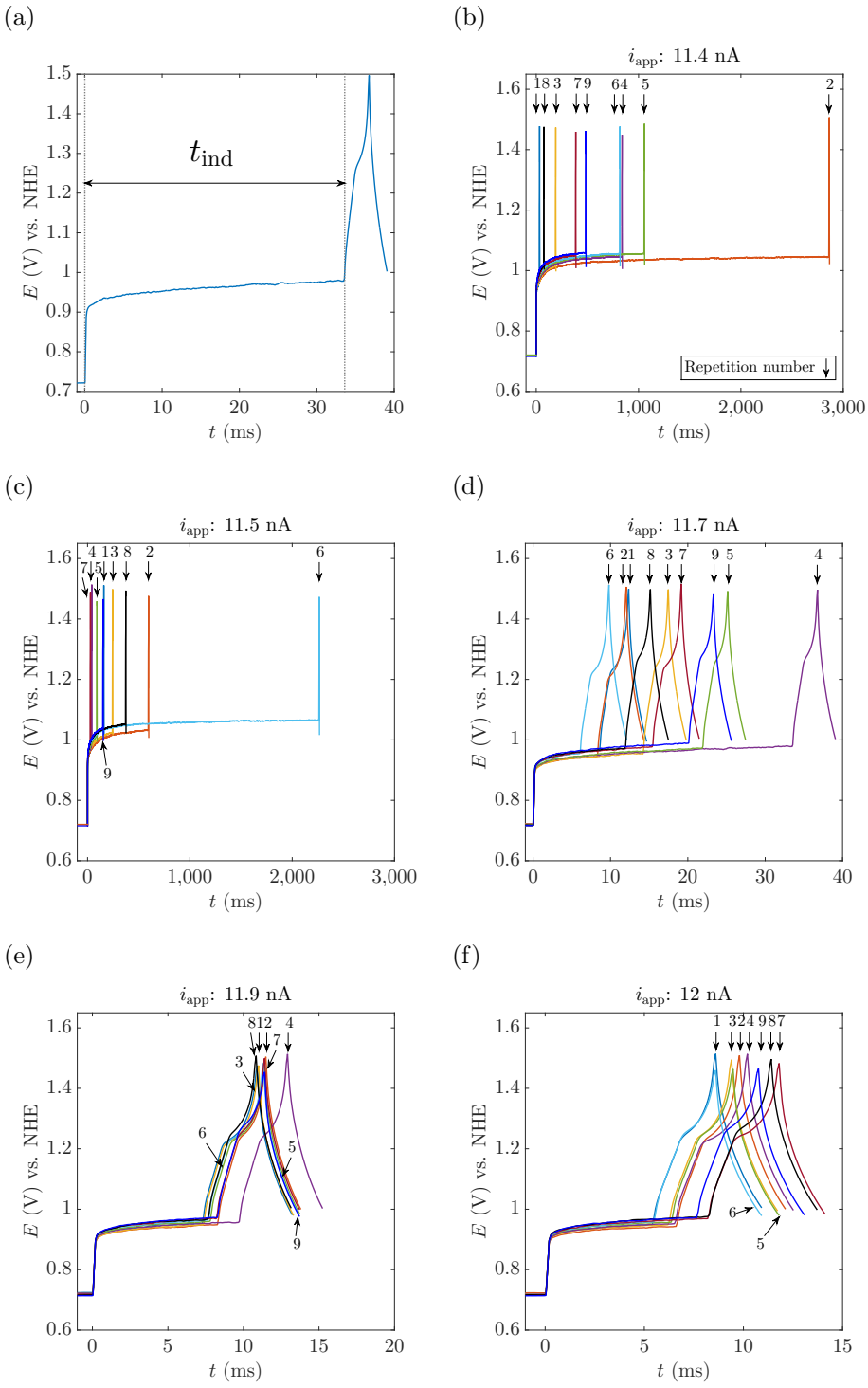

Figure S5: (a) Voltage-time plot during the nucleation of a nanobubble indicating how the nucleation time t_{ind} is measured. The current is stepped from 0 nA to i_{app} nA at 0 ms and returned to 0 nA after the electrode surface is blocked (b-f) Voltage-time plots used for measuring t_{ind} for a $a = 41$ nm electrode at different i_{app} (labelled). Note that different responses are plotted with different time scales. This figure is complementary to Figure 7 in the main text. The numbers indicate the sequence of the t_{ind} measured.

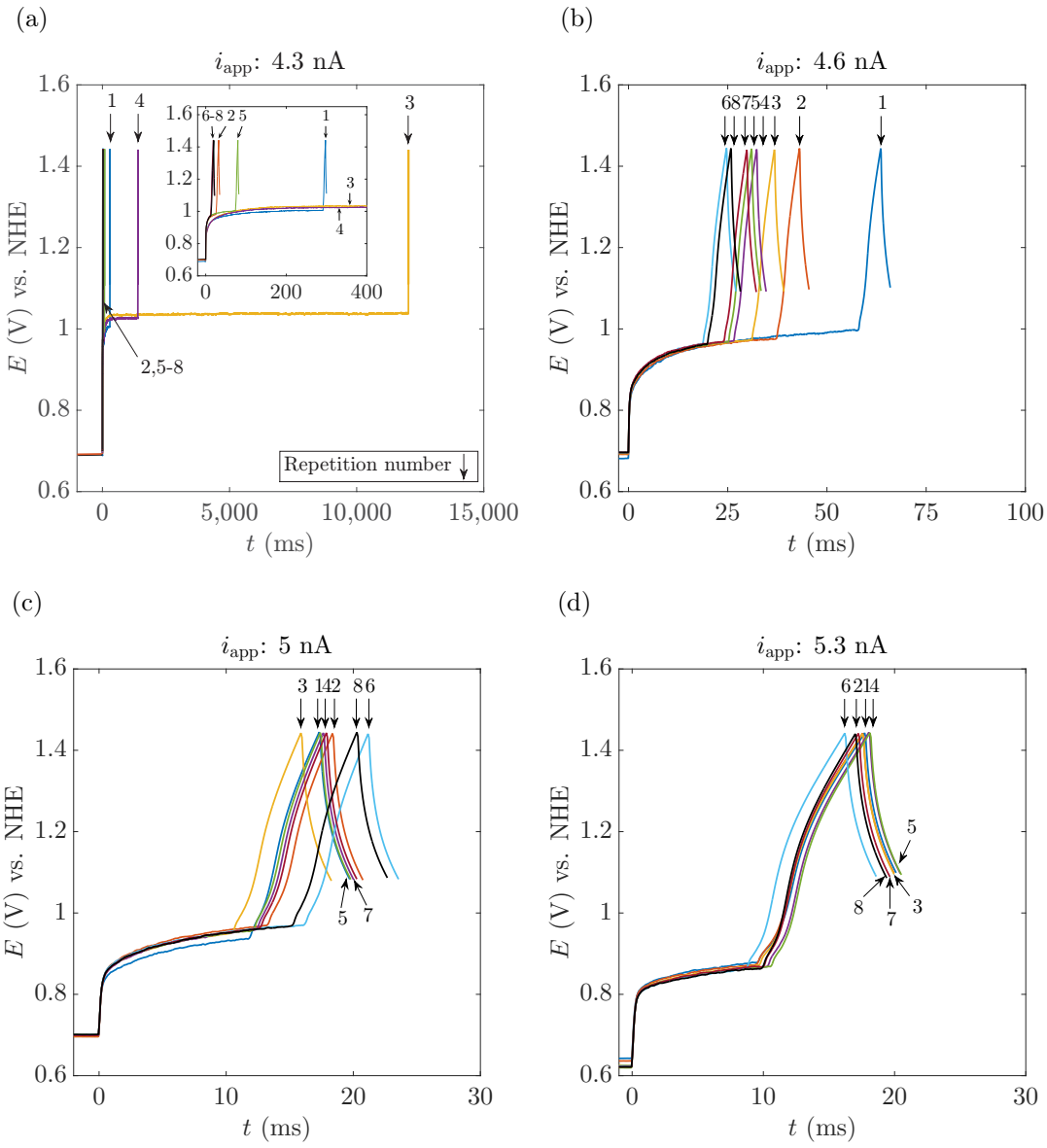

Figure S6: Voltage-time plots used to measure t_{ind} for multiple nucleation rate experiments performed at different i_{app} (labelled), corresponding to (a) $0.8i_{\text{nb}}^{\text{p}}$, (b) $0.85i_{\text{nb}}^{\text{p}}$, (c) $0.95i_{\text{nb}}^{\text{p}}$ and (d) i_{nb}^{p}. The electrode has an apparent radius of 3 nm. The numbers indicate the sequence of the t_{ind} measured. Note that different timescales are shown for the different applied currents.

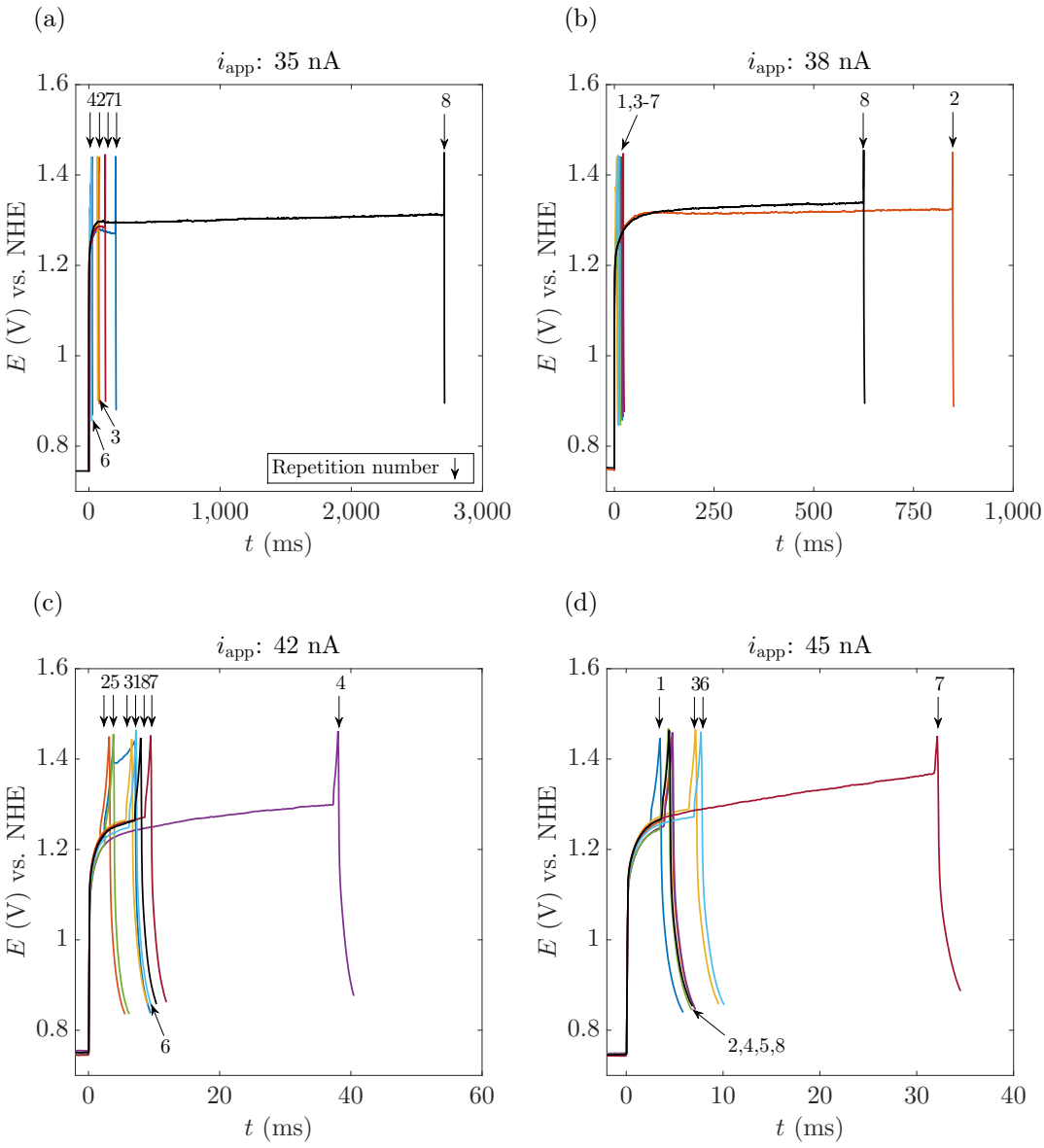

Figure S7: Voltage-time plots used to measure t_{ind} for multiple nucleation rate experiments performed at different i_{app} (labelled), corresponding to (a) $0.75i_{\mathrm{nb}}^{\mathrm{P}}$, (b) $0.85i_{\mathrm{nb}}^{\mathrm{P}}$, (c) $0.95i_{\mathrm{nb}}^{\mathrm{P}}$ and (d) $i_{\mathrm{nb}}^{\mathrm{P}}$. The electrode has an apparent radius of 51 nm. The numbers indicate the sequence of the t_{ind} measured. Note that different timescales are shown for the different applied currents.

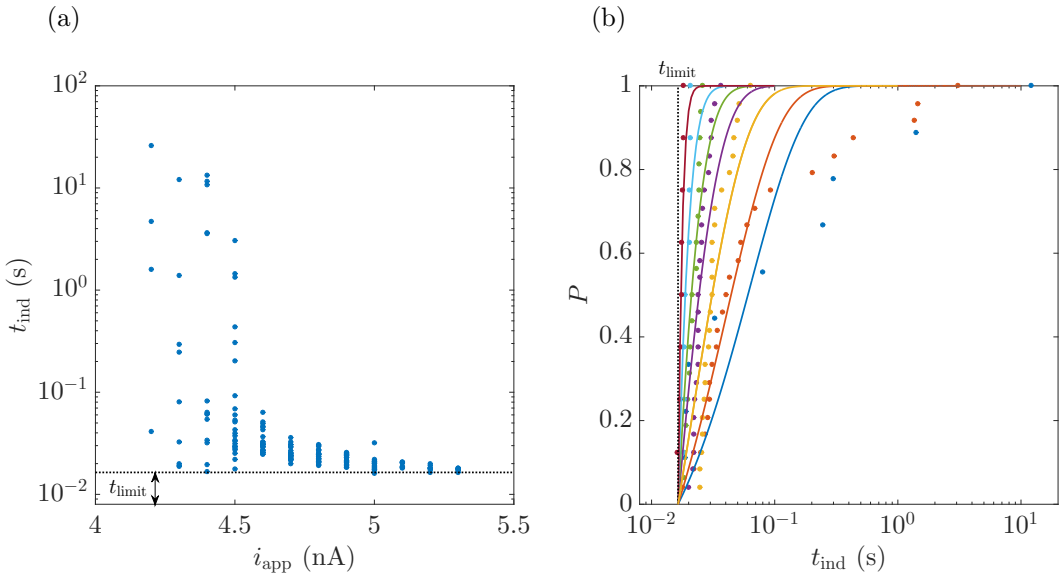

Figure S8: (a) Experimentally measured t_{ind} for different i_{app} at an electrode with apparent radius $a = 3$ nm. (b) Cumulative probability distribution P for nanobubble nucleation derived from the values of t_{ind} reported in panel (a) for different i_{app}. The theoretical curves correspond to the best fit using equation (1) in the main text. t_{lim} is the shortest accessible experimental time.

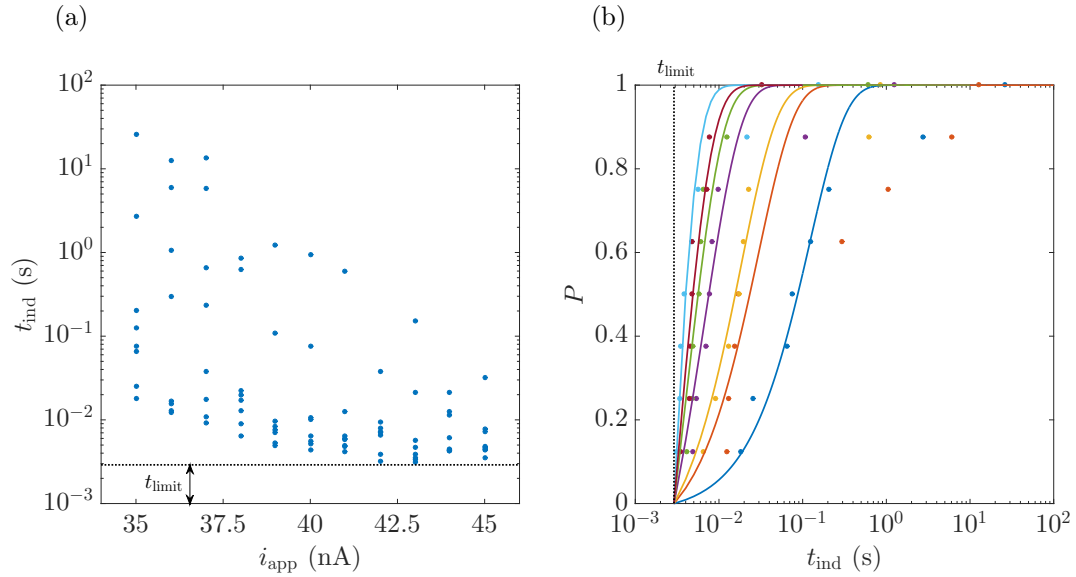

Figure S9: (a) Experimentally measured t_{ind} for different i_{app} at an electrode with apparent radius $a = 51$ nm. (b) Cumulative probability distribution P for nanobubble nucleation derived from the values of t_{ind} reported in panel (a) for different i_{app}. The theoretical curves correspond to the best fit using equation (1) in the main text. t_{lim} is the shortest accessible experimental time.

4. Bubble nucleation measurements without electrode surface conditioning

If the electrode surface is not conditioned before performing the nucleation rate experiments, large variability of $i_{\mathrm{nb}}^{\mathrm{p}}$ is observed (as shown in Figure 4d in the main text). In this case it is impossible to assure that we are measuring a stochastic nucleation time corresponding to i_{app}, since the nucleation time depends very sensitively on the proximity of the applied current i_{app} to $i_{\mathrm{nb}}^{\mathrm{p}}$. Voltage-time curves for bubble nucleation at a non-conditioned, $a = 6$ nm radius electrode are presented in Figure S10. In this example, the mean value of the measured nucleation times decreases systematically with increasing $i_{\mathrm{nb}}^{\mathrm{p}}$. However, the individual values are highly scattered with a very large mean deviation, thus indicating that these data do not correspond to a stochastic process.

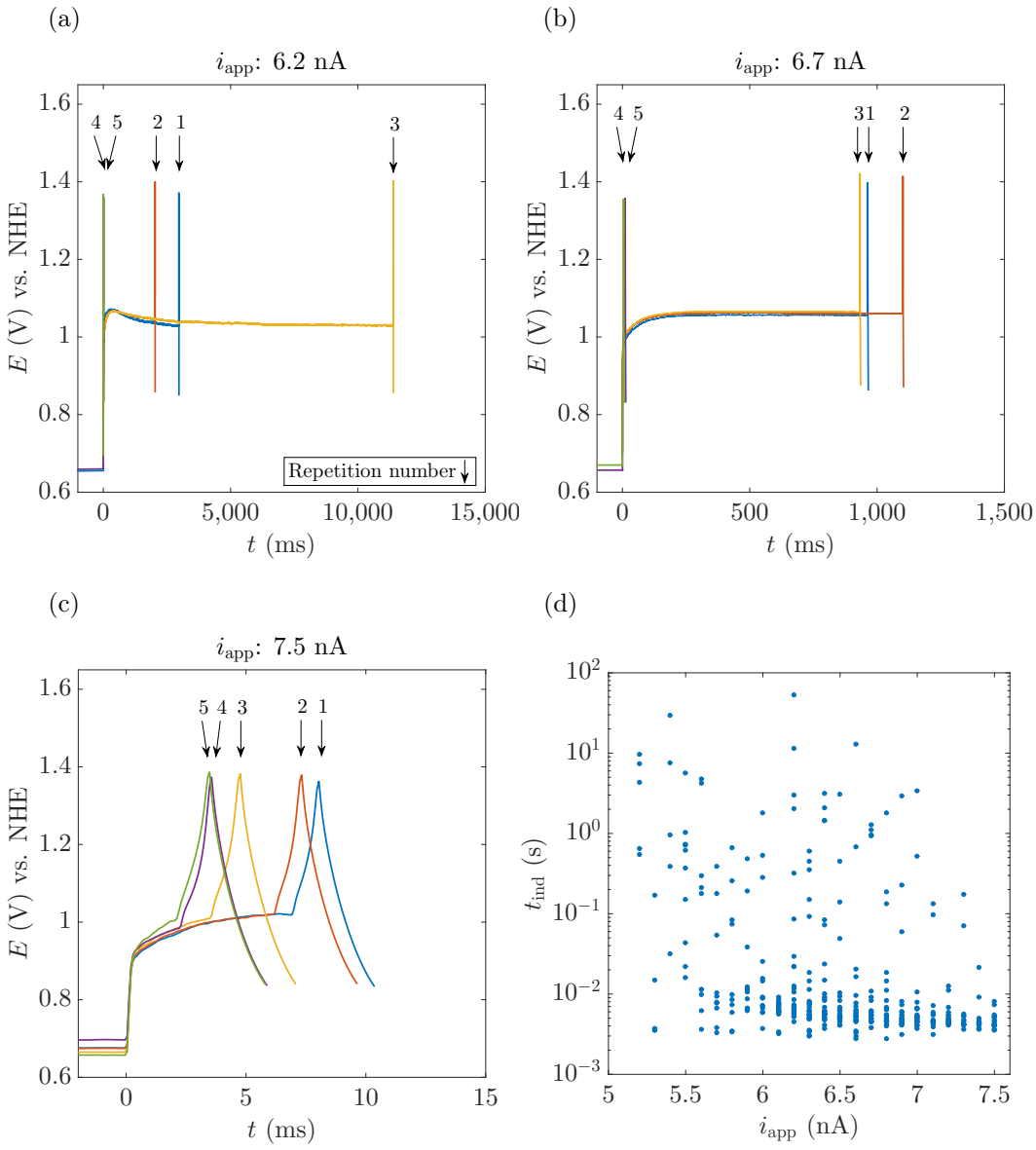

Figure S10: (a-c) Measurements of nanobubble nucleation time for increasing i_{app} on a non-conditioned, $a = 6$ radius nm electrode. (d) Scattered plot of nucleation times t_{ind} for different i_{app}. The scatter is so high that no proper probability analysis can be done. This is due to a changing i_{nb}^{p} from cycle to cycle, since the electrode surface has not been previously conditioned. The numbers on the arrows in (a)-(c) indicate the sequence of the t_{ind} measured.

References

(1) Zhang, B.; Galusha, J.; Shiozawa, P. G.; Wang, G.; Bergren, A. J.; Jones, R. M.; White, R. J.; Ervin, E. N.; Cauley, C. C.; White, H. S. Bench-top method for fabricating glass-sealed nanodisk electrodes, glass nanopore electrodes, and glass nanopore membranes of controlled size. *Anal. Chem.* **2007**, *79*, 4778–4787.

(2) Chen, Q.; Luo, L.; Faraji, H.; Feldberg, S. W.; White, H. S. Electrochemical measurements of single H_2 nanobubble nucleation and stability at Pt nanoelectrodes. *J. Phys. Chem. Lett.* **2014**, *5*, 3539–3544.

(3) German, S. R.; Edwards, M. A.; Chen, Q.; White, H. S. Laplace pressure of individual H_2 nanobubbles from pressure-addition electrochemistry. *Nano Lett.* **2016**, *16*, 6691–6694.

(4) Ren, H.; German, S. R.; Edwards, M. A.; Chen, Q.; White, H. S. Electrochemical generation of individual O_2 nanobubbles via H_2O_2 oxidation. *J. Phys. Chem. Lett.* **2017**, *8*, 2450–2454.

(5) Ma, W.; Hu, K.; Chen, Q.; Zhou, M.; Mirkin, M. V.; Bard, A. J. Electrochemical size measurement and characterization of electrodeposited platinum nanoparticles at nanometer resolution with Scanning Electrochemical Microscopy. *Nano Lett.* **2017**, *17*, 4354–4358.

(6) Wang, Y.; Rogers, E. I.; Compton, R. G. The measurement of the difussion coefficients of ferrocene and ferrocenium and their temperature dependence in acetonitrile using double potential step microdisk electrode chronoamperometry. *J. Electroanal. Chem.* **2010**, *648*, 15–19.

(7) Chen, Q.; Wiedenroth, H. S.; German, S. R.; White, H. S. Electrochemical nucleation of stable N_2 nanobubbles at Pt nanoelectrodes. *J. Am. Chem. Soc.* **2015**, *137*, 12064–12069.

(8) German, S. R.; Edwards, M. A.; Chen, Q.; Liu, Y.; Luo, L.; White, H. S. Electrochemistry of single nanobubbles. Estimating the critical size of bubble-forming nuclei for gas-evolving electrode reactions. *Faraday Discuss.* **2016**, *193*, 223–240.

(9) Katsounaros, I.; Schneider, W. B.; Meier, J. C.; Benedikt, U.; Biedermann, P. U.; Auer, A. A.; Mayrhofer, K. J. J. Hydrogen peroxide electrochemistry on platinum: towards understanding the oxygen reduction reaction mechanism. *Phys. Chem. Chem. Phys.* **2012**, *14*, 7384–7391.

(10) von Weber, A.; Baxter, E. T.; White, H. S.; Anderson, S. L. Cluster size controls branching between water and hydrogen peroxide production in electrochemical oxygen reduction at Pt_n/ITO. *J. Phys. Chem. C* **2015**, *119*, 11160–11170.

(11) German, S. R.; Edwards, M. A.; Ren, H.; White, H. S. Critical nuclei size, rate, and activation energy of H_2 gas nucleation. *J. Am. Chem. Soc.* **2018**, *140*, 4047–4053.